Control of Large-Scale Heat Transport by Small-Scale Mixing

PAOLA CESSI, W. R. YOUNG, AND JEFF A. POLTON

Scripps Institution of Oceanography, University of California, San Diego, La Jolla, California

(Manuscript received 9 June 2005, in final form 1 March 2006)

ABSTRACT

The equilibrium of an idealized flow driven at the surface by wind stress and rapid relaxation to nonuniform buoyancy is analyzed in terms of entropy production, mechanical energy balance, and heat transport. The flow is rapidly rotating, and dissipation is provided by bottom drag. Diabatic forcing is transmitted from the surface by isotropic diffusion of buoyancy. The domain is periodic so that zonal averaging provides a useful decomposition of the flow into mean and eddy components. The statistical equilibrium is characterized by quantities such as the lateral buoyancy flux and the thermocline depth; here, scaling laws are proposed for these quantities in terms of the external parameters. The scaling theory predicts relations between heat transport, thermocline depth, bottom drag, and diapycnal diffusivity, which are confirmed by numerical simulations. The authors find that the depth of the thermocline is independent of the diapycnal mixing to leading order, but depends on the bottom drag. This dependence arises because the mean stratification is due to a balance between the large-scale wind-driven heat transport and the heat transport due to baroclinic eddies. The eddies equilibrate at an amplitude that depends to leading order on the bottom drag. The net poleward heat transport is a residual between the mean and eddy heat transports. The size of this residual is determined by the details of the diapycnal diffusivity. If the diffusivity is uniform (as in laboratory experiments) then the heat transport is linearly proportional to the diffusivity. If a mixed layer is incorporated by greatly increasing the diffusivity in a thin surface layer then the net heat transport is dominated by the model mixed layer.

1. Introduction

In this study, we examine the role of mesoscale eddies and small-scale mixing in the poleward transport of heat, and in the maintenance of the oceanic thermocline. As an idealized model with some relevance to the Antarctic Circumpolar Current (ACC), we focus on domains that are periodic in the zonal direction. Forcing is provided by a surface wind stress $\tau_s(y)$ and by relaxation of the surface temperature toward a prescribed distribution $T_s(y)$. If $\tau_s dT_s/dy < 0$ (as in Fig. 1), then the wind stress generates an Ekman flow and an associated zonal-mean meridional circulation, $(\overline{v}, \overline{w})$, which tends to overturn the isopycnals. The meridional heat transport produced by this zonal-mean flow transports heat up the gradient of $T_s(y)$; that is, the heat flux $(\overline{v}\,\overline{T}, \overline{w}\,\overline{T})$ is cooling where $T_s(y)$ is a minimum and warming where $T_s(y)$ is a maximum.

It is easy to show using an entropy production argument that a steady wind stress such as $\tau_s(y)$ cannot coerce the ocean into transporting heat up the gradient of $T_s(y)$ (see section 5). Thus the divergence of the mean heat flux $(\overline{v}\,\overline{T}, \overline{w}\,\overline{T})$ must be canceled by a larger divergence[1] of the eddy heat flux, $(\overline{v'T'}, \overline{w'T'})$, so that the total ocean heat transport, mean plus eddy, is from the maximum of T_s to the minimum. Several recent studies have shown in detail how this cancellation occurs (Karsten et al. 2002; Marshall et al. 2002; Marshall and Radko 2003; Gallego et al. 2004; Kuo et al. 2005).

Using theories and diagnostics inspired by the transformed Eulerian mean formulation of Andrews and McIntyre (1976), these earlier works show that the competition between the mean heat flux and the eddy heat flux sets the structure of the zonally averaged temperature field $\overline{T}(y, z)$. A key ingredient, emphasized by Kuo et al. (2005), is that beneath a surface diabatic

Corresponding author address: Paola Cessi, 9500 Gilman Drive, University of California, San Diego, La Jolla, CA 92093-0213.
E-mail: pcessi@ucsd.edu

[1] Only the divergences cancel: there is not pointwise cancellation between $(\overline{v}\,\overline{T}, \overline{w}\,\overline{T})$ and $(\overline{v'T'}, \overline{w'T'})$. In the bulk of the thermocline the mean flux is vertical while the eddy flux lies along $\overline{T}(y, z)$ surfaces.

© 2006 American Meteorological Society

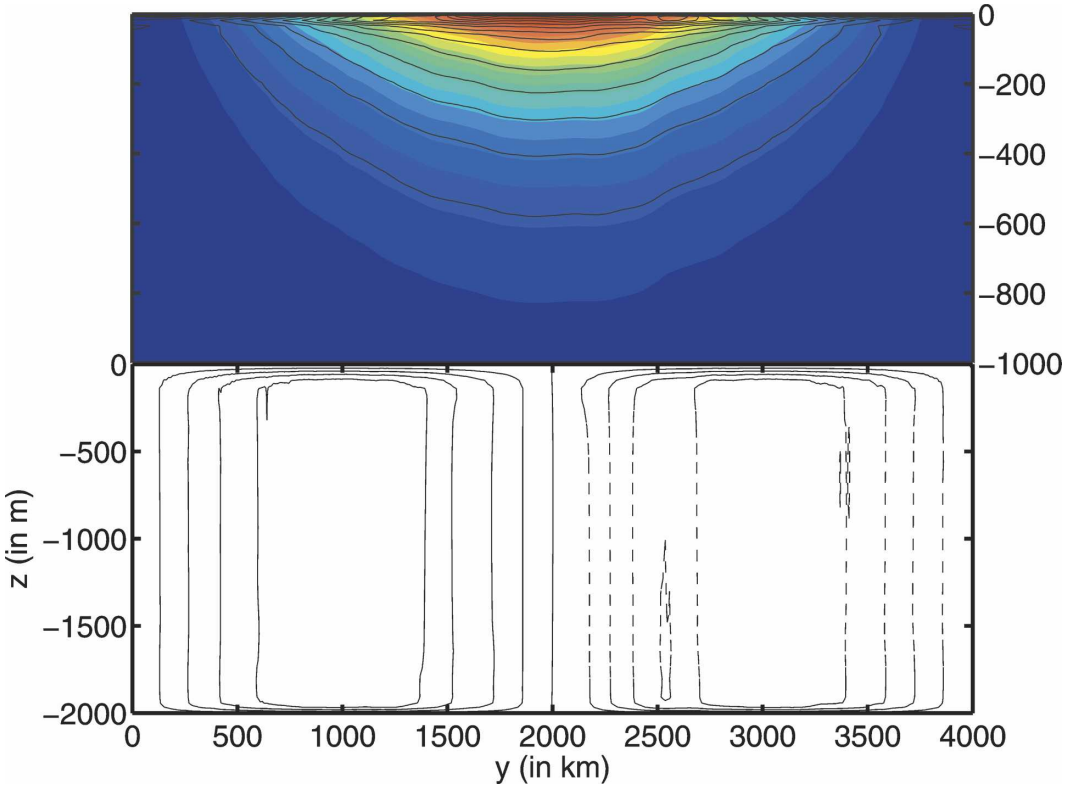

FIG. 1. (top) The zonally and time-averaged buoyancy, $\overline{b}(y, z)$, for Run 2 is shown in colors. The contour interval is 2×10^{-3} m^2 s^{-1}. The large scale Ertel potential vorticity, $\overline{b}_z(y, z)$, is shown in black. Below a surface trapped region, $\overline{b}$ and $\overline{b}_z$ are coincident. (bottom) The zonal mean streamfunction, $\overline{\psi}(y, z)$ is contoured (solid are positive and negative are dashed) and the contour interval is 2.1×10^{-1} m^2 s^{-1}.

layer (hereinafter SDL) the flow is nearly adiabatic, and the eddy fluxes of buoyancy lie along mean buoyancy surfaces; that is, the buoyancy flux is "skew." In these adiabatic interior layers, the potential vorticity is homogenized on mean buoyancy surfaces. The depth of the adiabatic homogenized thermocline is controlled by baroclinic instability and is largely independent of small-scale mixing; that is, independent of the mixing produced by breaking internal gravity waves.

In view of these important advances it seems that the adiabatic interior is well understood. However, it is the diabatic terms that determine the net heat transport (Andrews and McIntyre 1976), and in the ocean they are related to small-scale mixing. The dependence of small-scale mixing on the diffusivity κ is unknown because mixing depends on the vertical scale developed by temperature near the surface. The dependence of the heat flux on diffusivity and other nonconservative processes has not been discussed in the ACC literature cited above. We find that variations in diapycnal mixing affect the large-scale heat transport of simulations such as that in Fig. 1. We furthermore obtain a strong dependence of the net heat transport on the bottom drag. This result is not obvious since bottom drag affects directly the momentum budget, but not the heat balance. This sensitivity indicates that the size of the small residual between the mean and the eddies is crucially controlled by both bottom drag and diapycnal mixing.

Karsten et al. (2002) and Marshall et al. (2002) have emphasized that the cancellation between $\nabla \cdot (\overline{v}\overline{T}, \overline{w}\overline{T})$ and $\nabla \cdot (\overline{v'T'}, \overline{w'T'})$ is nearly complete. Kuo et al. (2005) show that the small residual circulation is almost zero below the SDL. Thus it is certainly possible that small-scale mixing has little effect on the depth of the main thermocline, but nonetheless plays an essential role within the SDL. Moreover, it is the depth of the SDL, rather than the depth of the thermocline, which determines the total efficacy of ocean heat transport. Consequently baroclinic eddy closure assumptions, which make no reference to small-scale mixing and bottom drag, can have little utility outside of the limited arena in which they are calibrated.

The role of diapcynal mixing and of a surface mixed layer in the large-scale heat transport were systematically examined by Gallego et al. (2004) in a zonally averaged model of the ACC, where eddy fluxes were

parameterized rather than computed. In that study the dependence of the meridional heat transport on the diapycnal diffusivity lead to very small residual heat transport (<0.1 PW) using observed values of mixing (1×10^{-5} m^2 s^{-1}). However, the meridional heat transport could be substantially enhanced by lateral transport in the model's mixed layer. Using models that resolve rather than parameterize eddies, we find qualitatively similar results to Gallego et al. (2004), although the quantitative dependence on parameters differs.

Our goal here is to obtain scaling estimates for the thermocline depth, the depth of the SDL, and for the net heat transport in terms of the external parameters (e.g., small-scale mixing, the strength of τ_s, the rotation rate). Although we systematically explore only the dependence on the diapycnal diffusivity and the bottom drag (the main source of energy dissipation), this is enough to constrain our scalings arguments.

2. The model

The model is

$$\begin{aligned} \frac{Du}{Dt} - fv + p_x &= \boldsymbol{\nabla}\cdot\nu\boldsymbol{\nabla}u + \delta_s^{-1}\gamma_s\tau_s - r\gamma_b u,\\ \frac{Dv}{Dt} + fu + p_y &= \boldsymbol{\nabla}\cdot\nu\boldsymbol{\nabla}v - r\gamma_b v,\\ p_z &= b,\\ \frac{Db}{Dt} &= \boldsymbol{\nabla}\cdot\kappa\boldsymbol{\nabla}b, \quad \text{and}\\ \boldsymbol{\nabla}\cdot\mathbf{v} &= 0. \end{aligned} \tag{1}$$

The velocity is $\mathbf{v} = (u, v, w)$ and the vertical coordinate is $-H < z < 0$, where H is the constant depth. The horizontal coordinates are $0 < x < L_x$ and $0 < y < L_y$. The buoyancy is $b = g\alpha T$.

We examine both a doubly periodic geometry, where periodicity is imposed in both the latitudinal as well as the longitudinal directions, and a channel geometry, where solid boundaries confine the flow meridionally. Although neither of these geometries apply realistically to the Southern Ocean, they both ensure that the system has closed budgets for mass, mechanical energy, and heat (as in Karsten et al. 2002; Kuo et al. 2005). Other approaches, directed at modeling the Southern Ocean (Marshall and Radko 2003; Olbers and Visbeck 2005), use an open boundary on the equatorward side of the domain. With an open lateral boundary it is difficult to relate directly the key processes maintaining the mean circulation and stratification to the surface heat fluxes. Thus, for an idealized process model we prefer to use a closed system and balance global budgets in terms of surface inputs and outputs.

a. Momentum forcing and bottom drag

The momentum equation is forced by a zonal surface stress concentrated near the surface $z = 0$. This wind stress is modeled with the body force in (1): $\delta_s^{-1}\gamma_s(z)\tau_s(y)\hat{\mathbf{x}}$. Here $\tau_s(y)$ is a specified pattern of wind stress and the constant $\delta_s \ll H$ is the depth of the surface layer. We use a sinusoidal wind profile

$$\tau_s(y) = -\tau \sin(2\pi y/L_y). \tag{2}$$

The nondimensional surface function,

$$\gamma_s(z) \equiv \sqrt{\frac{2}{\pi}} e^{-z^2/2\delta_s^2}, \tag{3}$$

tapers the body force smoothly to zero in the ocean interior. We use $\delta_s = 40$ m. The surface function γ_s is normalized so that

$$\int_{-H}^{0} \gamma_s(z)\, dz = \delta_s. \tag{4}$$

This normalization ensures that the total flux of zonal momentum into the water column is $\tau_s(y)$. Distributing the wind stress over a surface forced layer, with specified thickness δ_s, relieves the model from resolving Ekman layers.

The bottom stress is also represented as a body force $-r\gamma_b(z)(u\hat{\mathbf{x}} + v\hat{\mathbf{y}})$ in (1). This bottom drag force is applied over a layer of thickness $\delta_b \ll H$ using the bottom concentrated function

$$\gamma_b(z) \equiv \frac{H}{\delta_b}\sqrt{\frac{2}{\pi}} e^{-(z+H)^2/2\delta_b^2}. \tag{5}$$

We use $\delta_b = 40$ m. The time scale r^{-1} controls the strength of the bottom drag and is the spindown time of the barotropic velocities. Because the stresses are modeled as interior sources and sinks, the top and bottom boundary conditions are $\nu u_z = \nu v_z = 0$.

b. Buoyancy forcing

The thermal forcing at the surface $z = 0$ is applied with the restoring boundary condition

$$\delta_* b_z(x, y, 0, t) = b_s(y) - b(x, y, 0, t), \tag{6}$$

where $b_s(y)$ is the prescribed value toward which the surface buoyancy is restored; we use the sinusoidal profile:

$$b_s(y) = -B \cos(2\pi y/L_y). \tag{7}$$

The relaxation rate in (6) is controlled by the roughness length δ_*. The roughness length is related to the diffusivity by the relation $\delta_* = \kappa(0)C_p\rho/\lambda$, where λ (W m^{-2} K^{-1}) is the bulk transfer coefficient of heat (Haney

TABLE 1. The parameter values for the primitive equation model in the doubly periodic configuration are $H = 2000$ m, $L_x = 2 \times 10^6$ m, $L_y = 4 \times 10^6$ m, $f = 10^{-4}$ s^{-1}, $\tau = 10^{-4}$ m^2 s^{-2}, $B = 2 \times 10^{-2}$ m s^{-2}, and $P = 25$, $\Delta x = \Delta y = 10.417$ km.

Run	κ_a (m^2 s^{-1})	κ_s (m^2 s^{-1})	δ_* (m)	R (s^{-1})	H (m)	l (m)	D (m^2 s^{-1})	Symbol
1	8×10^{-4}	0	0	7.0×10^{-7}	499	79 256	573	×
2	8×10^{-5}	0	0	2.2×10^{-7}	213	149 885	164	×
3	2×10^{-5}	0	0	1.1×10^{-7}	146	165 231	84	×
4	2×10^{-5}	0	0	2.2×10^{-7}	180	131 739	71	×
5	8×10^{-5}	0	7.9	2.2×10^{-7}	221	149 002	151	▷
6	8×10^{-4}	6.3×10^{-2}	0	7.0×10^{-7}	611	75 034	804	+
7	8×10^{-5}	6.3×10^{-3}	0	2.2×10^{-7}	307	119 157	414	+
8	4×10^{-5}	3.1×10^{-3}	0	1.6×10^{-7}	279	129 223	325	+
9	2×10^{-5}	1.6×10^{-3}	0	1.1×10^{-7}	265	143 524	262	+
10	8×10^{-4}	1.6×10^{-3}	0	7.0×10^{-7}	563	86 030	634	○
11	8×10^{-5}	1.6×10^{-3}	0	2.2×10^{-7}	307	122 837	312	○
12	4×10^{-5}	1.6×10^{-3}	0	1.6×10^{-7}	290	125 445	263	○
13	8×10^{-4}	5.1×10^{-2}	0	1.0×10^{-6}	650	79 696	745	□
14	8×10^{-5}	6.3×10^{-3}	0	4.5×10^{-7}	377	105 185	342	□
15	4×10^{-5}	3.1×10^{-3}	0	2.2×10^{-7}	312	121 776	278	□
16	2×10^{-5}	1.6×10^{-3}	0	2.2×10^{-7}	320	119 384	207	□

1971), C_p is the specific heat, and ρ the density of water. Here we assume that λ is a constant. Using the typical value, $\lambda = 40$ W m^{-2} K^{-1}, we find that $1 < \delta_* < 100$ m for $1 \times 10^{-5} < \kappa(0) < 1 \times 10^{-3}$ m s^{-2}. In finite-difference models, the surface boundary condition (6) is equivalent to relaxing the buoyancy in the top model layer, of thickness dz_1, to $b_s(y)$ on a time scale $t_{\text{rlx}} = dz_1\delta_*/\kappa(0)$.

The ratio of δ_* to the depth of the thermocline determines whether the surface boundary condition (6) is effectively fixed flux or fixed buoyancy. The fixed buoyancy limit is obtained by taking $\delta_* = 0$. For heat, which is in turn related to temperature, this is the more relevant approximation.

Some earlier studies (Karsten et al. 2002; Kuo et al. 2005) impose the buoyancy flux over part of the ocean surface. This fixed-flux limit is obtained if both δ_* and $\kappa(0)b_s$ become large with the ratio $\kappa(0)b_s(y)/\delta_*$ fixed to the surface flux value. In this case the third term in (6) is negligible and the surface flux, $\kappa(0)b_z(x, y, 0, t)$, is proportional to $b_s(y)$. Equivalently, in a finite-difference formulation, the fixed-flux limit is obtained by taking the limit of $t_{\text{rlx}} \to \infty$, while keeping the ratio $b_s dz_1/t_{\text{rlx}}$ fixed. By making δ_* a function of horizontal position one can encompass variable boundary conditions such as those in the experiment of Karsten et al. (2002). The bottom boundary condition is no flux, $\kappa b_z(x, y, -H, t) = 0$.

c. Small-scale mixing

The eddy diffusivities $\nu(z)$ and $\kappa(z)$ represent small-scale mixing processes such as breaking internal gravity waves and mixed layer turbulence. As a simple model of enhanced diffusivity in the surface layer we use

$$\kappa(z) = \kappa_a + \kappa_s\gamma_s(z), \tag{8}$$

where $\gamma_s(z)$ is the Gaussian surface function in (3); $\kappa(z)$ represents small-scale mixing processes, such as breaking internal gravity waves and mixed layer turbulence. The constant κ_a is the small abyssal diffusivity and κ_s is the surface diffusivity that maintains the mixed layer. For the viscosity we take $\nu(z) = P\kappa(z)$, where the constant P is a Prandtl number.

d. Method of solution

The problem formulated in the previous section is solved with two different models. The first model is a finite difference primitive equation model in a doubly periodic domain, described in Cessi and Fantini (2004). The model resolves the vertical structures of γ_s and γ_b defined in (3) and (5). For all but one (Run 5 in Table 1) simulations with this model we take $\delta_* = 0$, so a fixed surface buoyancy condition is used.

The second model is the Massachusetts Institute of Technology (MIT) Ocean General Circulation Model (MITgcm; Marshall et al. 1997a,b), in a channel configuration. For this model, $\delta_s^{-1}\gamma_s = (dz_1)^{-1}\delta_{k,1}$ and $\gamma_b = (dz_N)^{-1}H\delta_{k,N}$, where $dz_1$and dz_N are the model's depths for the top and bottom layer, respectively, and $\delta_{k,J}$ is a Kronecker delta with unit value for level J and zero elsewhere. In other words, the wind and buoyancy forcing and the dissipation are concentrated in the top and bottom model level, respectively.

For this model δ_* is finite, but we typically operate in a regime where δ_* is much less than the vertical scale of the buoyancy. This is the regime where typical values are $t_{\text{rlx}} \leq 10$ days (using $dz_1 = 10$ m), and this is the fastest time scale in the mean buoyancy equation.

In summary, both models operate in or near the fixed surface buoyancy regime. In the oceanographic context, this is a more relevant regime than the fixed flux limit, when the tracer of interest is temperature (or heat). As discussed in Stommel (1961), the relaxation time for salinity is much longer than that for heat. Thus, the fixed-flux limit would be relevant for determining the vertical distribution of salinity.

3. The mean circulation and eddy buoyancy fluxes

We use an overbar to denote a zonal and time average:

$$\overline{A}(y, z) \equiv \int_0^{t_\infty} \int_0^{L_x} A(x, y, z, t) \frac{dx}{L_x} \frac{dt}{t_\infty}. \tag{9}$$

Here t_∞ is sufficiently long to remove the unsteadiness forced by eddy fluctuations. Angle brackets denote a volume and time average,

$$\langle A \rangle \equiv \int_0^{t_\infty} \int_{\mathcal{V}} A(x, y, z, t) \frac{dV}{\mathcal{V}} \frac{dt}{t_\infty}, \tag{10}$$

where the total volume of the model ocean is $\mathcal{V} = L_x L_y H$. A prime denotes the departure from the zonal and time average: $A'(x, y, z, t) \equiv A(x, y, z, t) - \overline{A}(y, z)$.

a. The mean circulation

Given $\overline{b}(y, z)$, one can obtain approximations to the zonal mean flow, $(\overline{u}, \overline{v}, \overline{w})$, by solving

$$\begin{aligned} -f\overline{v} &\approx \delta_s^{-1} \gamma_s(z) \tau_s(y) - r\gamma_b(z)\overline{u}, \\ f\overline{u} + \overline{p}_y &\approx 0, \\ \overline{p}_z &= \overline{b}, \quad \text{and} \\ \overline{v}_y + \overline{w}_z &= 0. \end{aligned} \tag{11}$$

Above, the Reynolds stresses, $(\overline{uv})_y$ and so on, are neglected. This is justified because the scales of motion, including eddies, are larger than the deformation radius. The bottom drag in the meridional momentum equation, $r\gamma_b\overline{v}$, is also neglected.

Integrating the zonal momentum equation from bottom to top we get

$$r \int_{-H}^{0} \gamma_b(z)\overline{u}(y, z)\, dz = \tau_s(y). \tag{12}$$

The left-hand side is simplified by replacing $\overline{u}(y, z)$ with $\overline{u}(y, -H)$. Using the normalization of $\gamma_b(z)$ in (4), one then has

$$\overline{u}_b(y) \approx \frac{\tau_s(y)}{rH}, \tag{13}$$

where $\overline{u}_b(y) \equiv \overline{u}(y, -H)$ is the zonal mean velocity at the bottom. With a flat bottom, the stress imposed at the top is balanced by frictional stresses at the bottom. This is certainly not the case in the oceanographic context, where form drag by bottom relief is the dominant form of momentum transfer to the solid earth. However, the zonal momentum budget will not be used in our scaling arguments.

The complete zonal mean velocity is then obtained by integrating the thermal wind relation vertically. One finds:

$$\overline{u}(y, z) \approx \frac{\tau_s(y)}{rH} - \frac{1}{f} \int_{-H}^{z} \overline{b}_y(y, \hat{z})\, d\hat{z}. \tag{14}$$

Figure 2 shows $\overline{u}$ for a typical calculation (Run 2 in Table 1): the barotropic component of the flow—the first term on the rhs of (14)—greatly exceeds the baroclinic component. We have verified that (14) is an accurate approximation for our numerical results.

Next, we obtain the mean meridional circulation. Introducing the zonal mean streamfunction $\overline{\psi}(y, z)$, defined by $(\overline{v}, \overline{w}) = (-\overline{\psi}_z, \overline{\psi}_y)$, we find from (11) that

$$\overline{\psi}(y, z) \approx -\frac{1}{f} \int_z^0 [\delta_s^{-1} \gamma_s(\hat{z}) - H^{-1}\gamma_b(\hat{z})]\, d\hat{z}\tau_s(y). \tag{15}$$

Outside the top and bottom layers, this simplifies to $\overline{\psi} \approx -f^{-1}\tau_s(y)$, or

$$\overline{v} = 0, \overline{w} \approx w_{\mathrm{Ek}}(y) \equiv -\frac{1}{f}\frac{d\tau_s}{dy}. \tag{16}$$

Above, $w_{\mathrm{Ek}}(y)$ is the Ekman pumping produced by the curl of $\tau_s(y)$.

b. Eddy buoyancy fluxes in the adiabatic interior

In the adiabatic interior the Ertel potential vorticity is homogenized (Kuo et al. 2005), and this implies that the eddy quasigeostrophic potential vorticity is zero—see the appendix and also Marshall et al. (1993). Additionally the scale of the eddies is larger than the Rossby radius. Thus from (A10) in the appendix:

$$\overline{v'b'} \approx \phi(y)\overline{b}_z. \tag{17}$$

Beneath the SDL the flow is almost adiabatic and consequently the eddy fluxes lie in the mean buoyancy surfaces, or

$$\overline{v'b'}\,\overline{b}_y + \overline{w'b'}\,\overline{b}_z \approx 0. \tag{18}$$

Combining (17) and (18) we obtain

$$\begin{pmatrix} \overline{v'b'} \\ \overline{w'b'} \end{pmatrix} \approx \begin{pmatrix} 0 & \phi \\ -\phi & 0 \end{pmatrix} \begin{pmatrix} \overline{b}_y \\ \overline{b}_z \end{pmatrix}. \tag{19}$$

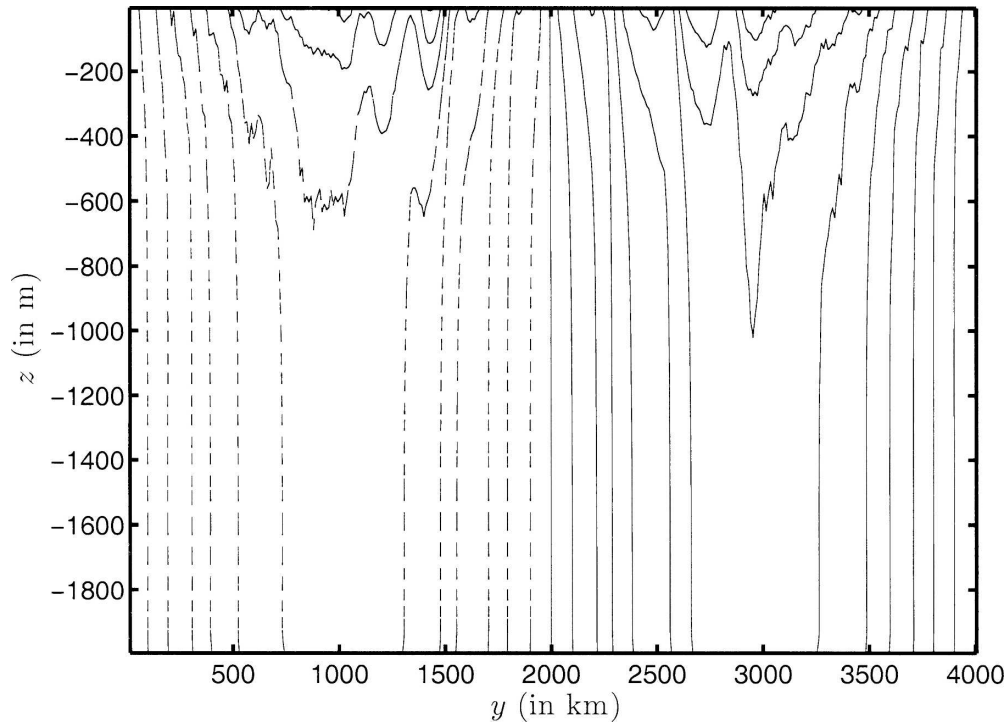

FIG. 2. The time- and zonally averaged zonal flow, $\overline{u}$, for run 2 is contoured as a function of y and z. The contour interval is 0.01 m s^{-1} and negative values are dashed.

Thus the function $\phi(y)$ in (17) is identified as the interior antisymmetric eddy diffusion; $\phi(y)$ is also the "quasi Stokes streamfunction" of Plumb and Ferrari (2005).

In the adiabatic interior layers $\overline{v} = 0$ and the mean buoyancy equation reduces to

$$(\overline{v'b'})_y + (\overline{w'b'})_z + \overline{w}\overline{b}_z \approx 0, \tag{20}$$

where $\overline{w} \approx w_E(y) = -f^{-1}d\tau_s/dy$ is the Ekman velocity in (16). Substituting (19) into (20) gives

$$\phi(y) \approx f^{-1}\tau_s(y). \tag{21}$$

The rhs of (21) is just $-\overline{\psi}$, so $\overline{\psi} + \phi \approx 0$. Thus, as emphasized by earlier investigators, within the adiabatic interior there is almost total cancellation between the mean streamfunction and the quasi Stokes streamfunction (Karsten et al. 2002; Marshall et al. 2002; Gallego et al. 2004; Kuo et al. 2005). This cancellation is quite apparent when the eddy and mean component of the buoyancy fluxes are compared. Figure 3 shows the vertically integrated meridional fluxes (top) and the horizontally integrated vertical fluxes (bottom). For both components, the net buoyancy flux is much smaller than the separate mean and eddy components, which largely cancel except within the SDL.

The vanishing of the residual streamfunction, $\phi + \overline{\psi}$, is a consequence of the homogenization of potential vorticity on isopycnals and the adiabaticity of the interior region. Both conditions are found to hold in more complicated models of the Antarctic Circumpolar Cur-

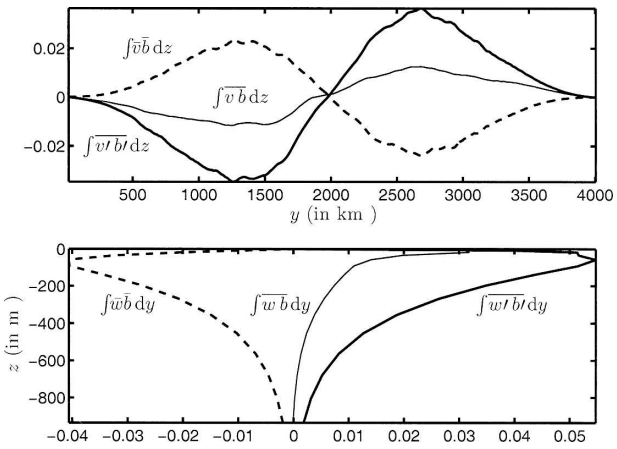

FIG. 3. (top) The vertically integrated meridional transport of buoyancy is plotted as a function of y (thin solid) for run 2 in Table 1. The transports by the zonally averaged circulation (dashed) and by the eddies (thick solid) are also shown, and they are much larger than their sum. (bottom) The meridionally integrated vertical transport of buoyancy is plotted as a function of z (thin solid). The transports by the zonally averaged circulation (dashed) and by the eddies (thick solid) are also shown, and they are much larger than their sum except in the mixed layer.

rent that include realistic forcings and geometry (e.g., Marshall et al. 1993). From another perspective, the result, $\overline{v'b'}/\overline{b}_z = \tau_s/f$, is Johnson and Bryden's (1989) momentum balance in which the eddy form stress transmits eastward momentum downward.

c. The mean stratification

A popular approach to determining the mean stratification $\overline{b}(y, z)$ is to follow Green (1970) and posit an eddy closure relation $\overline{v'b'} = -\kappa_{\text{eddy}}\overline{b}_y$ (Johnson and Bryden 1989; Karsten et al. 2002; Marshall and Radko 2003; Olbers and Visbeck 2005). Various prescriptions for κ_{eddy} have been used in the literature. Combining this eddy diffusion closure with the relations in the previous section leads to a first-order hyperbolic equation for $\overline{b}$. With the surface boundary condition in (7) and a constant κ_{eddy}, the solution of this hyperbolic equation produces a quite unrealistic mean stratification. Thus, instead of pursuing this approach we propose the exponential thermocline

$$b_{\text{int}}(y, z) \equiv -B + A(y)e^{z/h} \tag{22}$$

as a phenomenological representation of the mean stratification in the adiabatic interior. With suitable adjustment of the thermocline depth h and of the function $A(y)$, the exponential model (22) provides a good fit to the observed interior stratification.

Although the exponential model has little theoretical basis, it does have several features that make $b_{\text{int}}(y, z)$ useful for scale analysis. First, $\partial_z b_{\text{int}} = h^{-1}(b_{\text{int}} + B)$ so that $b_{\text{int}}(y, z)$ has homogenized potential vorticity. Second, $b_{\text{int}}(-H, z) = -B$; that is, the fluid is unstratified beneath the densest point on the surface.

The function $A(y)$ is determined by applying the surface boundary condition in (6). However, for $\delta_* \sim h$, the boundary condition cannot be applied directly to the expression (22) because there is a correction in the SDL, which changes the surface derivative of $\overline{b}$, although the correction to the function itself is small. We will have more to say about this in section 7. In the limit of $\delta_* \ll h$, the surface boundary condition can be applied without knowledge of the SDL correction, and to a good approximation $A(y) = b_s + B$.

4. The mechanical energy balance

To obtain a scaling for the thermocline depth, and for the net heat transport, we first need to establish some results concerning the mechanical energy balance.

Dotting $\mathbf{v}$ into the momentum equations and averaging over the volume gives the global kinetic energy budget:

$$\delta_s^{-1}\langle\gamma_s\tau_s u\rangle + \langle wb\rangle = r\langle\gamma_b|\mathbf{v}|^2\rangle + \langle\nu\|\nabla\mathbf{v}\|^2\rangle. \tag{23}$$

Following Paparella and Young (2002) we obtain a more convenient expression for the total conversion between kinetic and potential energy, $\langle wb\rangle$. Multiplying the buoyancy equation by z and volume averaging we obtain

$$\langle wb\rangle = \langle\kappa\overline{b}_z\rangle. \tag{24}$$

The no-flux bottom boundary condition,

$$\kappa(-H)b_z(x, y, -H, t) = 0,$$

is used crucially in the proof of (24). Equation (24) shows that the two terms on the rhs of $\langle wb\rangle = \langle\overline{w}\overline{b} + \overline{w'b'}\rangle$ almost cancel, leaving a small positive residual of order κ.

Using (24) to eliminate $\langle wb\rangle$ in (23), the mechanical energy equation can be rewritten exactly as

$$\delta_s^{-1}\langle\gamma_s\tau_s\overline{u}\rangle + \langle\kappa\overline{b}_z\rangle = r\langle\gamma_b|\mathbf{v}|^2\rangle + \langle\nu\|\nabla\mathbf{v}\|^2\rangle. \tag{25}$$

The first term on the rhs of (25) is the dissipation of mechanical energy by bottom drag. This is the main sink of mechanical energy and is always larger than the dissipation of mechanical energy by internal friction, $\langle\nu\|\nabla\mathbf{v}\|^2\rangle = \langle\nu(u_x^2 + u_y^2 + u_z^2 + v_x^2 + v_y^2 + v_y^2)\rangle$. Thus, we neglect the final term in (25) and the dominant balance in the mechanical energy budget is

$$H^{-1}\langle\tau_s\overline{u}_0\rangle \approx r\langle|\mathbf{v}_b|^2\rangle, \tag{26}$$

where $\overline{u}_0(y) \equiv \overline{u}(y, 0)$ is the zonal mean flow at the top, $z = 0$, and $\mathbf{v}_b(x, y, t) \equiv \mathbf{v}(x, y, -H, t)$ is the total (mean plus eddy) bottom velocity.[2]

In passing from (25) to (26) we also neglected the conversion from potential energy, that is, the term $\langle\kappa\overline{b}_z\rangle$. To appreciate this approximation we can make some order-of-magnitude estimates. Typical values for the wind work are

$$H^{-1}\langle\tau_s\overline{u}_0\rangle = O(2.5 \times 10^{-8}\ \text{m}^2\ \text{s}^{-3}), \tag{27}$$

where we have used $\tau_s \sim 10^{-4}\ \text{m}^2\ \text{s}^{-2}$, $\overline{u}_0 \approx 0.5\ \text{m}\ \text{s}^{-1}$ and $H = 2000$ m. To estimate the conversion from potential energy, take $\kappa \approx 10^{-4}\ \text{m}^2\ \text{s}^{-1}$ and $\overline{b}_z \approx 10^{-6}\ \text{s}^{-2}$ so that

$$\langle\kappa\overline{b}_z\rangle = O(10^{-10}\ \text{m}^2\ \text{s}^{-3}). \tag{28}$$

Thus the nonuniform surface buoyancy $b_s(y)$ does not provide a substantial source of mechanical energy in (26): the total mechanical energy balance shows that the flow is entirely driven by the wind work $H^{-1}\langle\tau_s\overline{u}_0\rangle$.

From a wider perspective, this illustrates the hypoth-

[2] In passing from (25) to (26) we have also made the mild approximation of replacing $\mathbf{v}$ with surface and bottom values within the relevant δ_s and δ_b boundary layers.

esis of Munk and Wunsch (1998) that the main physical energy inputs to the ocean circulation are wind stress and tides. Dewar et al. (2005, manuscript submitted to *J. Mar. Res.*) have recently argued that biology provides a third energy source comparable in order of magnitude the physical sources identified by Munk and Wunsch. In these energy budgets, conversion from potential energy, that is, $\langle wb \rangle$, is inconsequential because of the identity (24) (Paparella and Young 2002).

Now from (14), the zonal mean flow at the surface is

$$\overline{u}_0 \approx \overline{u}_b - \frac{1}{f}\int_{-H}^{0} \overline{b}_y(y, z)\, dz, \tag{29}$$

where $\overline{u}_b(y) \approx \tau_s(y)/rH$ is the zonal mean flow at the bottom. Thus the wind work is

$$\langle \tau_s \overline{u}_0 \rangle \approx rH\langle \overline{u}_b^2 \rangle - \left\langle \int_{-H}^{0} \overline{b}(y, z)\, dz \cdot w_E(y) \right\rangle. \tag{30}$$

Above, $w_E(y) = -f^{-1}d\tau_s/dy$ is the Ekman velocity. The final term in (30), which is much smaller than the other two, is the "useful wind work." This is the net energy extracted from the wind after bottom drag on $\overline{u}$—that is, $rH\langle \overline{u}_b^2 \rangle$—dissipates most of the wind work. This small amount of power is all that is available to drive the baroclinic eddies against bottom drag.

Substituting (30) into (26) we obtain[3] the key result

$$-H^{-1}\left\langle \int_{-H}^{0} \overline{b}(y, z)\, dz \cdot w_E(y) \right\rangle \approx r\langle |\boldsymbol{u}_b'|^2 \rangle. \tag{31}$$

Thus the dominant balance in (31) is between the useful wind work and the bottom dissipation by the eddies. Later we use this approximation to estimate the magnitude of the barotropic eddy velocities in terms of $\overline{b}$.

Because of the large numerical cancellation in passing from (26) to (31), it is important to verify that the conversion from potential energy, $\langle \kappa b_z \rangle$ is still much smaller than the remaining terms in (31). Using $L_y \approx 6 \times 10^6$ m as the meridional scale of $\tau_s(y)$, and the numerical values from our earlier estimates, we find that the order of magnitude of the useful wind work is

$$H^{-1}\left\langle \int_{-H}^{0} \overline{b}(y, z)\, dz \cdot w_E(y) \right\rangle = O(10^{-9}\ \mathrm{m^2\ s^{-3}}). \tag{32}$$

The useful wind work estimated above is smaller by a factor of 25 than the total wind work estimated in (27), but still greater by a factor of 10 than the conversion from potential energy in (28) [and (28) uses a generously large κ].

The balance in (31) is the situation described by Gill et al. (1974): on the left-hand side available potential energy is generated by Ekman pumping. This energy is transferred via baroclinic instability to mesoscale eddies. The right-hand side of (31) is the damping of the baroclinically driven eddies by bottom drag. Notice that in order to understand the energetics of the eddy field one can deal with the mean Eulerian velocity, $w_E(y)$, rather than the residual velocities obtained from the transformed Eulerian mean formulation.

An alternative derivation of useful wind work

To better understand (31) we now give a second derivation, which applies in an arbitrary geometry, including bottom topography and nonzero β. This derivation does not rely on the explicit expression of the mean zonal wind given by (13). The first point to note is that (24) is unchanged provided that there is no flux of buoyancy through the bottom (in this more general context angle brackets denote a total volume and time average over the basin).

Because zonal averaging is no longer possible, one makes a Reynolds decomposition $\mathbf{v}(x, y, z, t) = \overline{\mathbf{v}}(x, y, z) + \mathbf{v}'(x, y, z, t)$ based on a time average and the assumption of a spectral gap. One readily obtains the mean,

$$\sum_{i=1,2}\sum_{j=1,3} \langle u_i' u_j' \partial_{x_j} \overline{u}_i \rangle + \delta_s^{-1}\langle \gamma_s \tau_s \overline{u} \rangle + \langle \overline{w}\overline{b} \rangle = r\langle \gamma_b |\overline{u}|^2 \rangle, \tag{33}$$

and eddy,

$$-\sum_{i=1,2}\sum_{j=1,3} \langle u_i' u_j' \partial_{x_j} \overline{u}_i \rangle + \langle w'b' \rangle = r\langle \gamma_b |\mathbf{v}'|^2 \rangle, \tag{34}$$

contributions to the energy budget. In the Reynolds stress terms, we have used the notation $(x_1, x_2, x_3) = (x, y, z)$ and $(u_1, u_2, u_3) = (u, v, w)$. Notice that triple correlation terms vanish under the total volume average within angle brackets and that, summing (33) and (34), we recover the total energy budget in (23).

The first terms on the lhs of (33) and (34) are the Reynolds stress conversions between the mean and the eddies. To the extent that Reynolds stress work is negligible in the eddy equation we obtain $\langle w'b' \rangle \approx r\langle \gamma_b |\mathbf{v}'|^2 \rangle$. Using (24), $\langle w'b' \rangle \approx -\langle \overline{w}\overline{b} \rangle$ we obtain

$$-\langle \overline{w}\overline{b} \rangle \approx r\langle \gamma_b |\mathbf{v}'|^2 \rangle. \tag{35}$$

[3] We neglect the small amount of energy dissipated by bottom drag on $\overline{v}$.

In this general context[4] we cannot make the final step that $\overline{w}(x, y, z) \approx w_E(y)$, so we do not totally recover (31) from (35). Yet the derivation of (35) is useful as an illustration of the two assumptions: (i) the existence of a spectral gap and (ii) negligible Reynolds stress work in the eddy energy budget, which are required to justify the balance between generation of APE and eddy dissipation proposed by Gill et al. (1974).

5. Entropy production and heat transport

In this section we develop some integral constraints on large-scale heat flux. All of our deductions are kinematic in the sense that we use only the buoyancy equation

$$\frac{Db}{Dt} = \nabla \cdot \kappa \nabla b, \tag{36}$$

and the boundary condition (6). Thus the results apply to both the model formulated in the previous section and to laboratory experiments such as those of Karsten et al. (2002). The main difference in interpretation is that in the numerical model $\kappa(z)$ parameterizes small-scale mixing, whereas in the laboratory experiment the constant κ is the molecular diffusion of heat.

With constant salinity, as in the present model, the meridional heat flux is $\rho_0 c_p Q(y)/(g\alpha)$, where g is gravity, α is the coefficient of thermal expansion, and $Q(y)$ is defined by

$$HQ(y) \equiv \int_{-H}^{0} \overline{vb} - \kappa \overline{b}_y \, dz. \tag{37}$$

Averaging the buoyancy equation (36) in the zonal and vertical directions gives

$$H \frac{dQ}{dy} = F_0. \tag{38}$$

On the right-hand side above,

$$F_0(y) \equiv \kappa_0 \overline{b}_{z0}, \tag{39}$$

where subscript 0 indicates evaluation at the surface $z = 0$, for example; $b_{z0} \equiv b_z(x, y, 0, t)$. The heat flux between the atmosphere and the ocean (watts per square meter) is $\rho C_p F_0/(g\alpha)$.

To obtain the entropy production budget, multiply (36) by b and average over the volume. Using the restoring boundary condition in (6), the result is

$$\chi = H^{-1} \langle b_s F_0 \rangle, \tag{40}$$

where

$$\chi \equiv \langle \kappa |\nabla b|^2 \rangle + \kappa_0 \frac{\delta_*}{H} \langle b_{z0}^2 \rangle. \tag{41}$$

Above, angle brackets represent the volume–time average defined in (10) and χ is regarded as the total production of entropy by small-scale mixing processes. The first term on the rhs of (41) is the interior production of b^2, the model analog to the entropy production by molecular diffusion.[5] The final term in (41) is the production of b^2 associated with the restoring surface boundary condition. In the fixed-temperature limit ($\delta_* \to 0$), the surface production vanishes. In the fixed-flux limit ($\delta_* \to \infty$, with fixed $\kappa_0 b_s/\delta_*$) the surface production also vanishes.

Using (38) to eliminate $F_0(y)$ from (40), we obtain a key constraint on the unknown flux function $Q(y)$:

$$\left\langle Q \frac{db_s}{dy} \right\rangle = -\chi < 0. \tag{42}$$

The right-hand side of (42) is negative so that on average the flux $Q(y)$ and the gradient of the surface buoyancy forcing, db_s/dy, have opposite signs. Thus the wind stress cannot coerce the ocean to transport heat up the surface temperature gradient everywhere.

Our goal is to relate the flux function $Q(y)$ to the imposed surface forcing $b_s(y)$ and $\tau_s(y)$. The simplest assumption is a diffusive closure

$$Q \approx -D \frac{db_s}{dy}. \tag{43}$$

This heuristic argument combined with (42) motivates the definition of the large-scale diffusivity D as

$$\left\langle \left(\frac{db_s}{dy} \right)^2 \right\rangle D \equiv \chi. \tag{44}$$

We use D defined above as a convenient index of the heat transport of the ocean. In Fig. 4 we compare $Q(y)$ to $-D\mathrm{d}b_s/dy$ for one of our computations (Run 2 in Table 1). The agreement between the computed and diagnosed heat fluxes is good except that the former is concentrated in regions narrower than those predicted by the diffusive closure, a feature shared by all computations. We emphasize that D defined in (44) is a measure of the bulk residual transport in the system. Here D is a residual quantity, and will generally be much less

[4] With β and basin geometry, the large-scale vorticity balance $\beta v = f w_z$ implies that $\overline{w}$ depends on z.

[5] An alternative interpretation, which avoids mentioning entropy, is that (40) is the production–dissipation balance of b^2 stuff. This is similar to familiar buoyancy variance arguments, although (40) is the budget for the total b^2, rather than just the buoyancy variance b'^2.

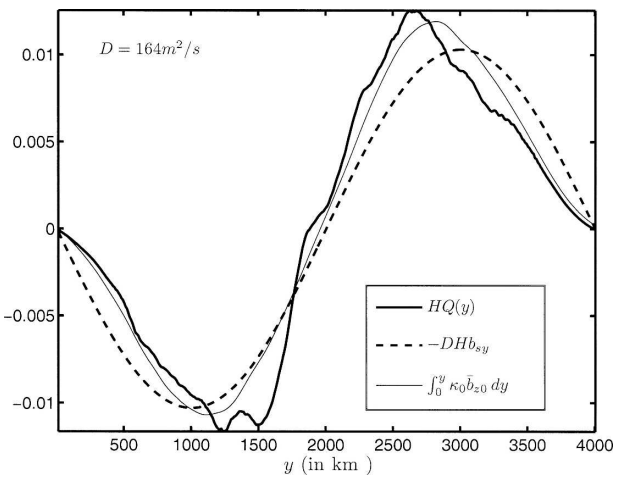

FIG. 4. The vertically integrated meridional transport of buoyancy, $HQ(y)$, (solid) is compared with the diffusive closure, $-HDdb_s/dy$ (dashed) for run 2 in Table 1. Also plotted is the surface flux F_0 (thin solid), which should equal $HQ(y)$ in statistical steady state.

than the baroclinic eddy diffusivity. Because (40) requires a two-dimensional surface integral, rather than a three-dimensional volume integral, it is more convenient to diagnose χ and D from the entropy power integral in (40), rather than the definition in (41).

6. The adiabatic interior and the thermocline depth

a. A scale estimate of the thermocline depth h

We denote the depth of the homogenized, adiabatic thermocline by h and relate h to other variables by assuming that all three terms in the buoyancy equation,

$$(\overline{v'b'})_y + (\overline{w'b'})_z + \overline{w}\overline{b}_z \approx 0, \tag{45}$$

have the same order of magnitude. Several earlier investigators have assumed that $(\overline{w'b'})_z$ is negligible so that there is further simplification in (45) to a two-term balance between $(\overline{v'b'})_y$ and $\overline{w}\overline{b}_z$ [see the discussion surrounding (8) in Kuo et al. (2005)]. Thus we begin by explaining why we believe that there must be a full three-term balance.

Integrating (45) across the domain, the divergence $(\overline{v'b'})_y$ vanishes and using (16) we obtain

$$\frac{d}{dz}\int_0^{L_y} \overline{w'b'}\, dy = \int_0^{L_y} \frac{1}{f}\frac{d\tau_s}{dy}\,\overline{b}_z\, dy\,. \tag{46}$$

The right-hand side is strongly nonzero and positive because both $d\tau_s/dy$ and $\overline{b}_z$ are proportional to $\cos(2\pi y/L_y)$. More fundamentally, the useful wind work on the left-hand side of (31) is obtained if one multiplies (46) by z and integrates over the volume of the fluid. Thus in order to supply energy to the baroclinic eddies the right hand side of (46) must be nonzero.

Earlier works, which neglect $(\overline{w'b'})_z$ in (45), assume quasigeostrophic scaling so that $\overline{b}_z$ is dominantly a function of z only. In this case the rhs of (46) would indeed integrate to zero. However, we find that the amplitude of the "basic stratification,"

$$\tilde{b}(z) \equiv L_y^{-1}\int_0^{L_y} \overline{b}(y, z)\, dy, \tag{47}$$

is comparable to the meridional buoyancy differences left in $\overline{b}(y, z) - \tilde{b}(z)$. The exponential model (22) illustrates this zonally averaged buoyancy structure: $\overline{b}(y, z)$ has the same range of values in the vertical and meridional directions. Thus, although the Rossby number is small, quasigeostrophic scaling cannot be applied to the zonally averaged buoyancy, while it can be applied to the eddies (e.g., Pedlosky 1987, section 6.24). These arguments, which apply with equal force to a closed cylindrical geometry such as Karsten et al. (2002), show that the vertical flux $\overline{w'b'}$ must be important in (45) to balance the horizontal integral of $\overline{w}\overline{b}_z$.

To apply scale analysis, we must find an independent scaling $\overline{v'b'}$, and thus we introduce

$$V^2 \equiv \langle v_b'^2 \rangle, \tag{48}$$

where $v_b'(x, y, t)$ is barotropic component of $v'(x, y, z, t)$. We use V as an estimate of a typical eddy velocity. As argued more extensively in Cessi and Fantini (2004), the horizontal advection of buoyancy is dominated by the barotropic component of the velocity. This is because, by thermal wind balance, the baroclinic component of the horizontal velocity is largely orthogonal to the buoyancy gradient. We also introduce the mixing length, l, defined by

$$l^2 \equiv \langle b'^2 \rangle / \langle \overline{b}_y^2 \rangle. \tag{49}$$

Using l and the domain scale L_y there is a scale separation parameter

$$\epsilon \equiv l/L_y. \tag{50}$$

Here l is the length over which the changes in b' are comparable to those in $\overline{b}$; that is, $L_y|\nabla b'| \sim B$, where B is strength of the surface buoyancy forcing in (7).

The mean buoyancy and mean vertical velocity are estimated as

$$\overline{b} \sim B \quad \text{and} \quad \overline{w} \sim \frac{\tau}{fL_y}, \tag{51}$$

where τ and B are the surface forcing parameters in (2) and (7). Because $\overline{b}$ and b' share the same vertical scale,

namely, h, balancing the second and third terms in (20) gives

$$b' \sim \epsilon B, w' \sim \frac{\tau}{\epsilon f L_y}. \tag{52}$$

Notice that $w' \approx \overline{w}/\epsilon \gg \overline{w}$: this is why $\overline{w'b'}$ in (45) is comparable to the other two terms.

Equation (31) shows that the eddies are driven against bottom drag by the useful wind work $\langle w_E \overline{b} \rangle$. To estimate the volume average $\langle w_E \overline{b} \rangle$ we must keep in mind that the correlation is nonzero only over the thermocline, of thickness h, and not over the whole depth of the fluid. Thus

$$\langle w_E \overline{b} \rangle \sim \frac{h}{H} w_E \overline{b} \sim \frac{h}{H} \frac{\tau B}{f L_y}. \tag{53}$$

With the estimate above, the eddy velocity scale V is estimated using (31) as

$$\frac{h}{H} \frac{\tau B}{f L_y} \sim r V^2. \tag{54}$$

From (17) and (21) we have $\overline{v'b'} \approx \tau_s \overline{b}_z / f$, and this relation provides another scale estimate for V:

$$V \sim \frac{\tau L_y}{l f h}. \tag{55}$$

Eliminating V between (54) and (55) we find

$$h \sim L_y \left(\frac{r H \tau}{f B l^2} \right)^{1/3}. \tag{56}$$

We can also express the barotropic eddy velocity V as

$$V \sim \frac{\tau}{f l} \left(\frac{f B l^2}{r H \tau} \right)^{1/3}. \tag{57}$$

Our attempt to relate h and V to external parameters is not completely successful because the mixing length l in (56) and (57) is unknown. However, we can anticipate that l, usually associated with the energy-containing scale of the barotropic eddies (Larichev and Held 1995; Smith et al. 2002; Riviere et al. 2004; Thompson and Young 2006), will decrease as the bottom drag, r, increases. This is because bottom drag arrests the inverse cascade that accompanies the equilibration of the barotropic eddies (Rhines 1977; Salmon 1980). Indeed, in a flat-bottom, f-plane geometry bottom drag is the only mechanism that can prevent eddies to expand to the domain size, L_y. If this is true, then we anticipate that h will have a dependence on r steeper than the 1/3 power law explicitly identified in (56).

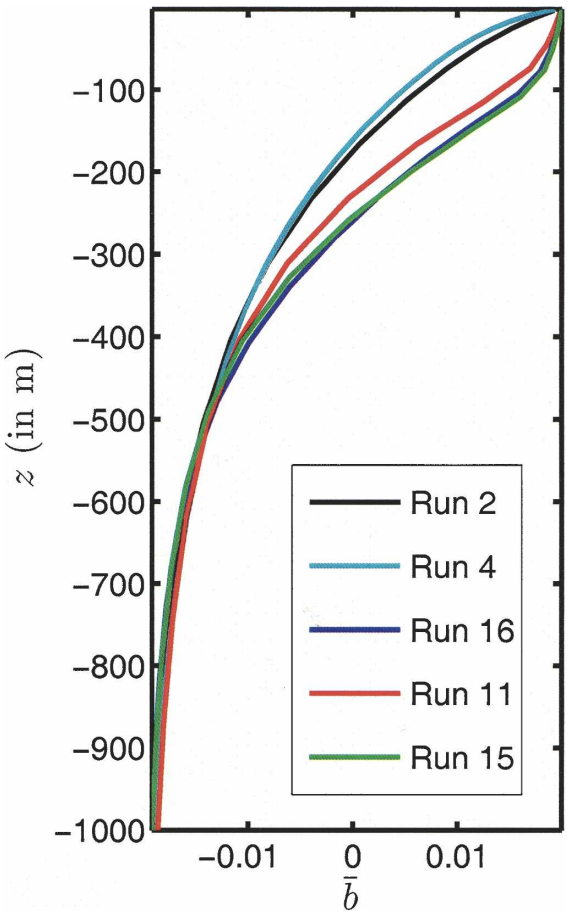

FIG. 5. The vertical profiles of $\overline{b}(L_y/2, z)$ are shown for five computations listed in Table 1; all share the same value of r and runs 2 and 4 have $\kappa_s = 0$.

b. Comparison with simulations

As a practical measure of the thermocline depth h we use

$$h^2 \equiv \langle (\overline{b} - \tilde{b})^2 \rangle / \langle (\overline{b} - \tilde{b})_z^2 \rangle, \tag{58}$$

where the basic stratification $\tilde{b}(z)$ is defined in (47). The definition (58) is easy to apply diagnostically to model results. Moreover, (58) gives exactly the depth of the thermocline if the vertical structure of $\overline{b}$ decreases exponentially from the surface, with $\overline{b}(y, z) - \tilde{b}(z) \propto b_s(y) \exp(z/h)$. Figure 5 shows the vertical profiles of $\overline{b}$ at $y = L_y/2$ for five computations (cf. Table 1) that share the same value of the bottom drag, r, but have different values of κ_a or κ_s. Below the mixed layer, when present, all profiles show an approximate exponential decay. And if the vertical shape of $\overline{b} - \tilde{b}$ is not precisely exponential, then the diagnostic definition (58) should still roughly coincide with scaling estimates

TABLE 2. The parameter values for the MITgcm model in the channel configuration are $H = 2000$ m, $L_x = 2 \times 10^6$ m, $L_y = 2 \times 10^6$ m, $\Delta x = \Delta y = 15.625$ km, $f = 10^{-4}$ s^{-1}, $\tau = 10^{-4}$ m^2 s^{-2}, $B = 2 \times 10^{-2}$ m s^{-2}, and $\kappa_s = 0$. The shapes of the wind stress and buoyancy forcings are given by $\tau_s(y) = -\tau \sin(\pi y/L_y)$ and $b_s(y) = -B \cos(\pi y/L_y)$, respectively.

Run	κ_a (m^2 s^{-1})	P	δ_*(m)	R (s^{-1})	H (m)	L (m)	D (m^2 s^{-1})	Symbol
17	8×10^{-5}	25	7.1	2.2×10^{-7}	250	231 000	146	◊
18	2×10^{-5}	50	0.6	1.1×10^{-7}	187	287 000	100	◊

of the thermocline depth. The values of h reported in Tables 1 and 2 are calculated using (58).

For those calculations in Table 1 where the diffusivity is increased in a near-surface mixed layer (runs 6–16), it is appropriate to measure h not from the surface, but from the bottom of the mixed layer, $z = -h_{\text{mix}}$. We define the bottom of the mixed layer as the depth at which the diffusivity in (8) reaches 2 times the abyssal value:

$$h_{\text{mix}} \equiv \delta_s \sqrt{2 \log(\sqrt{2/\pi}\kappa_s/\kappa_a)}. \tag{59}$$

Figure 6 (top) shows $h - h_{\text{mix}}$ as a function of r for all the calculations in Tables 1 and 2. Figure 6 shows that $h - h_{\text{mix}}$ depends on r but not on κ (which was the other parameter varied). All calculations in Table 1 collapse on a line with a slope of $\sqrt{r}$, with the exception of those with the highest value of κ_a and r for which the adiabatic interior approximation fails.[6] Figure 6 (bottom) shows l, defined in (49) as a function of r, and all calculations collapse on a line of slope $r^{-1/4}$, consistent with the notion that bottom drag arrests the inverse cascade of the barotropic eddies. These slopes are in quantitative agreement with the scaling in (56): $h \propto r^{1/3} l^{-2/3} \propto r^{1/3} (r^{-1/4})^{-2/3} = r^{1/2}$. Calculations using the MITgcm (Table 2) show the same dependencies of h and l on r as the doubly periodic runs of Table 1, though the values of h and l are larger. We do not attribute these differences to the choice of $\delta_* \neq 0$ in the boundary condition (6) since runs 5 and 17 share all parameter values, including δ_*, except for the numerical implementation (cf. Tables 1 and 2). We hypothesize that the alternative numerical solution techniques and spatial resolutions are to blame. Nevertheless, the fit of all the data to the proposed scalings, even across numerical models, is encouraging.

c. Comparison with other scaling estimates of h

Several numerical and laboratory experiments before ours have proposed scalings of the thermocline depth h in idealized channel geometries. All of these works, including the present, share the assumption of a quasi-adiabatic interior where the mean and eddy buoyancy fluxes balance. These assumptions lead to the scaling relation $\overline{v'b'} \approx \tau B/fh$. This relation can also be obtained from Johnson and Bryden's (1989) zonal momentum balance. Moreover, all are unified by a common interpretation of the eddy fluxes of buoyancy in terms of an eddy closure of the form $\overline{v'b'} \approx (Vl) \times (B/L_y)$. Combining the scaling relations above one obtains

$$h \sim \frac{\tau L_y}{fVl}. \tag{60}$$

The difference among these works resides in estimating the transfer velocity, V, and the mixing length, l, in (60).

The interpretation of the laboratory and numerical experiments of Karsten et al. (2002), Marshall and Radko (2003), Cenedese et al. (2004) revolves around arguments originally presented by Green (1970). Green's assumption is that the eddy transfer velocity,

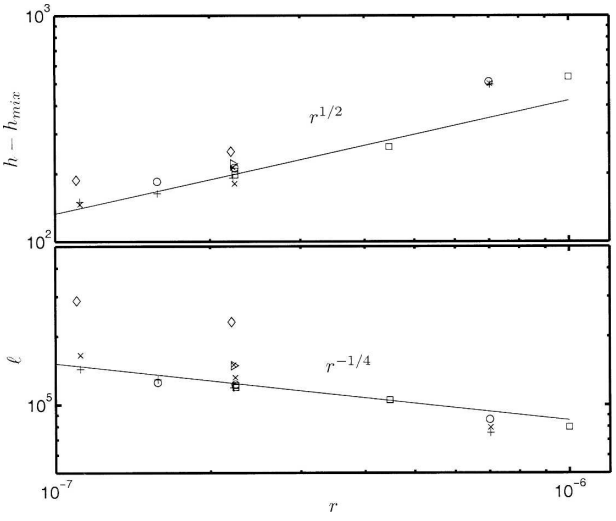

FIG. 6. (top) The vertical scale (m) of the zonally averaged buoyancy, defined in (58) as a function of the bottom drag r (s^{-1}), for all runs of Table 1. For runs 6–16 the thickness of the mixed layer, $h_{\text{mix}} = \delta_s \sqrt{2 \log(\sqrt{2/\pi}\kappa_a/\kappa_s)}$, is subtracted from h. The continuous line shows a slope $r^{1/2}$. (bottom) The mixing length, l, defined in (49) is plotted as a function of r for all the runs in Table 2. The continuous line shows a slope $r^{-1/4}$, which is in quantitative agreement with the scaling (56).

[6] The exceptional points falling above the line in Fig. 6 (top) are runs 1, 6, and 10.

V, scales with the baroclinic component of the zonally averaged zonal velocity, that is, $\overline{u} - \overline{u}_b$ in (13) and (14). Thus $V \sim Bh/(fL_y)$. The mixing length is taken as the external horizontal scale of the zonal flow, $l \sim L_y$. Putting these estimates into (60), Marshall and his collaborators obtain for the depth of the thermocline $h \approx \sqrt{\tau L_y/B}$.

The calculations of Henning and Vallis (2005) retain the dependence of the Coriolis parameter on latitude, $f = f_0 + \beta y$, and include bottom relief, while our work is on the f plane and has a flat bottom. Henning and Vallis (2005)'s estimate of Vl in (60) stems from ideas rooted in the geostrophic turbulence literature. Thus, as in our (48), Henning and Vallis (2005) assume that the eddy transfer velocity, V, is that of the barotropic eddies. Henning and Vallis (2005) make an equipartition assumption that the barotropic eddy kinetic energy is of the same magnitude as the eddy available potential energy: $V \sim (Bh)^{1/2} l/L_y$. The mixing length is associated with the largest eddy scale, identified with the Rhines scale, so that $l \sim (V/\beta)^{1/2}$. The resulting scaling for the depth of the thermocline is $h \sim (\tau L_y^2 f)^{2/5} B^{-3/5}$. The implicit assumption of Henning and Vallis (2005) is that β is the dominant mechanism to arrest the inverse cascade. Thus, in contrast to our view, the barotropic eddies are assumed to equilibrate at an amplitude independent of the explicit dissipation parameters, such as the bottom drag.

Our approach to estimating the eddy flux is also inspired by ideas from geostrophic turbulence theory, and we follow Henning and Vallis (2005) and Cessi and Fantini (2004) in identifying V as the barotropic eddy velocity. However, our numerical calculations do not support the assumption of equipartition of eddy energy between the baroclinic and barotropic modes. Instead we use the energy balance argument of section 4 to estimate the eddy transfer velocity V; this inevitably introduces the bottom drag r. Furthermore, our computations do not support the inertial hypothesis of Kolmogorov, so we cannot use the arguments summarized in Smith et al. (2002) to estimate the drag-induced halting scale, and unfortunately l remains unknown. Finally we have proposed an objective definition of the mixing length l in (49). Diagnosis of l using this definition indicates that the mixing length is considerably smaller than the domain scale L_y, but larger than the deformation radius.

7. The buoyancy transport for constant κ

In (56) we related the thermocline depth, h, to the external parameters and to the mixing length l. The goal of this section is to relate the bulk diffusivity, D in (44), to the external parameters. The determination of D is equivalent to finding the surface buoyancy flux [cf. (40) and (44)]. Because in all our computations the surface buoyancy forcing is close (or equal) to the fixed buoyancy limit, the amplitude of the buoyancy field is known and of order B, but the surface flux, and thus the net meridional heat transport, is unknown.

We first discuss the case with $\kappa_s = 0$ in (8); that is, the small-scale diffusivity $\kappa(z)$ is uniform and equal to the small abyssal value κ_a. In the next section we turn to the case with $\kappa_s \gg \kappa_a$.

The scaling hypothesis developed in this section and the next is that the mean buoyancy field has the structure

$$\overline{b}(y,z) = b_{\rm int}\left(\frac{y}{L_y}, \frac{z}{h}\right) + \frac{d}{h} b_{\rm sdl}\left(\frac{y}{L_y}, \frac{z}{d}\right), \qquad (61)$$

where $d \ll h$ is the depth of the SDL; d is defined more precisely below in (66). In (61), both functions $b_{\rm int}$ and $b_{\rm sdl}$ vary by $O(B)$ as their arguments range over the domain; $b_{\rm int}$ is the buoyancy in the adiabatic interior, defined in (22), while $b_{\rm sdl}$ is the boundary layer modification that is limited to the SDL; that is, if $|z|/d \to \infty$, then $b_{\rm sdl} \to 0$.

Thus the change in $\overline{b}$ across the SDL produced by the function $b_{\rm sdl}$ is of order $d/h \ll 1$. So most of the structure in the mean buoyancy field is carried by the function $b_{\rm int}$, which is a creature of the adiabatic interior. However the boundary layer function $b_{\rm sdl}$ does produce a change in $\overline{b}_z$ of order B/h, which is of the same magnitude as the contribution from $b_{\rm int}$. Thus we can roughly say that in the regime where the buoyancy is fixed at the surface, there is not a significant SDL boundary layer in $\overline{b}$, but that there is a significant SDL boundary layer in $\overline{b}_z$. We now substantiate these assertions and their implications for heat transport with diagnosis of the simulations and scaling arguments.

With reference to Fig. 5 it is clear that the constant κ simulations (runs 1–4) do not have a boundary layer in $\overline{b}$ near the surface. Thus, we can make a scale estimate of the buoyancy flux at the sea surface at the surface as

$$F_0 \equiv \kappa_a \overline{b}_{z0} \sim \kappa_a B/h. \qquad (62)$$

Given the relation $\langle b_{\rm sy}^2 \rangle D = H^{-1} \langle b_s F_0 \rangle$ from section 5, we can use (62) to estimate that

$$D \sim \frac{\kappa_a L_y^2}{hH}. \qquad (63)$$

Since h is independent of κ_a, (63) predicts that the net transport of buoyancy (and thus of heat) is linearly proportional to κ_a. In particular the buoyancy transport Q, defined in (37), is

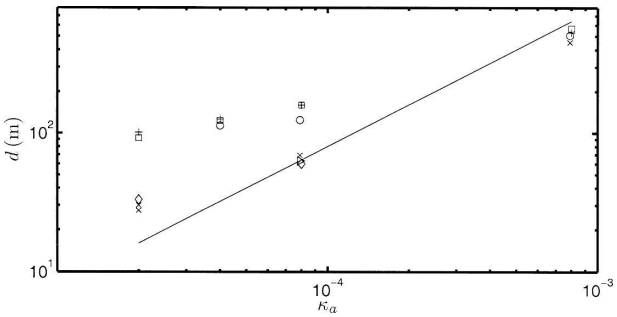

FIG. 7. The vertical scale (m) of the depth at which the cumulative meridional transport [(37)] reaches 1% of its maximum value is plotted as a function of κ_a for all of the runs in Table 1. The solid line has a slope unity and indicates $d \propto \kappa_a^1$.

$$HQ \approx -DH\frac{db_s}{dy} \sim \frac{\kappa_a L_y B}{h}. \tag{64}$$

The scaling relation (63) and (64) are confirmed by the numerical calculation presented in Fig. 8. For the calculations with constant diffusivity ($\times$ symbol), Dh has a clear linear dependence on κ_a. Because h is independent of κ_a, this implies that D depends linearly on κ_a. We plot the product Dh in Fig. 8 because h does depend on the bottom drag r. Thus if r is increased so that the thermocline deepens, then the heat transport index D must decrease to compensate. Runs 3 and 4 in Fig. 8 confirm this prediction. They have the same value of $\kappa_a = 2 \times 10^{-5}$ and different values of r: they produce the same Dh in Fig. 8.

Now we inquire where the bulk of the heat transport takes place. Is the heat flux carried throughout the thermocline, concentrated within the diabatic surface layer, or equipartitioned between the interior and the near-surface regions? We define the cumulative entropy production as

$$\hat{\chi}(z) \equiv -H^{-1}L_y^{-1}\int_0^{L_y}\frac{db_s}{dy}\left(\int_{-H}^{z}\overline{vb} - \kappa\bar{b}_y\,dz\right)dy. \tag{65}$$

The identity (42) shows that $\hat{\chi}(0) = \chi$. We determine the depth, d, to which significant transport occurs as the value of z where $\hat{\chi}$ reaches 1% if its maximum χ (achieved at the surface). That is

$$\hat{\chi}(-d) = 0.01\chi, \text{ (definition of } d). \tag{66}$$

Figure 7 shows d as a function of κ_a for the computations listed in Tables 1 and 2. The crosses denote runs without enhanced surface mixing, and d clearly decreases with κ_a: the solid line in Fig. 7 has a slope of unity and indicates $d \propto \kappa_a$. If the bulk of the transport occurred in the thermocline, then d should be proportional to h and thus depend on the bottom drag, r, rather than on κ_a, but this is not the case. In the following we argue that, if the meridional heat transport occurs effectively within the SDL, then d should scale linearly with κ_a.

Integrating the buoyancy equation from $z = -d$ to the surface we find

$$\partial_y\int_{-d}^{0}\overline{vb}\,dz - \overline{wb}|_{z=-d} = F_0 - \kappa\bar{b}_z|_{z=-d}. \tag{67}$$

We write $\overline{vb} = -\bar{\psi}_z\bar{b} + \overline{v'b'}$. Integrating by parts and using (15), (19), and (21), the balance (67) simplifies to

$$\partial_y\left[\int_{-d}^{0}(\overline{\psi b}_z + \overline{v'b'})\,dz\right] = F_0 - \kappa\bar{b}_z|_{z=-d}. \tag{68}$$

By definition, d is the deep boundary of the diabatic region, and thus the diffusive flux at $z = -d$ is much smaller than the surface flux, F_0: we can neglect the final term in (68). Notice also that at $z = -d$ the integrand in the first term is virtually zero. Thus both sides of (68) are insensitive to the exact location of $z = -d$. A similar argument was used by Kuo et al. (2005) to estimate the heat budget in the SDL.

To estimate the two remaining terms in (68) we assume that $\overline{v'b'}$ does not have a boundary layer enhancement as the surface is approached. This property is clearly illustrated in the bottom panel of Fig. 3. In other words, the assumption is that eddy transports are of the same amplitude within the surface layer as in the adiabatic interior. Within the SDL the precise cancellation between $\overline{\psi b}_z$ and $\overline{v'b'}$, characteristic of the adiabatic interior, does not occur. This is not surprising, given that the eddy transport of buoyancy is effected by the barotropic eddies. We can thus assume that $\overline{v'b'}$ has the same amplitude from the surface to the thermocline and estimate the left-hand side of (68) to be $O[d\tau B/(fhL_y)]$. Because the mean buoyancy field does not exhibit a change in vertical scale as the surface is approached, we can estimate the right side $F_0 \sim \kappa_a B/h$. Combining these estimates we find that

$$d \sim \frac{\kappa_a f L_y}{\tau}. \tag{69}$$

The constant κ runs in Fig. 7 (indicated by $\times$) support the prediction in (69). At the smallest value of κ_a the points fall above the prediction (69). However, with $\kappa_a = 2 \times 10^{-5}$ m^2 s^{-1} it is difficult to resolve the small-scale structure of the vertical derivative correction to b_{sdl}.

8. The buoyancy transport for enhanced surface small-scale mixing

We turn now to the case in which diffusion is augmented near the surface; that is, $\kappa_s \gg \kappa_a$ (8). This case

is easier, both analytically and numerically. The mean buoyancy field $\overline{b}$ still has the structure in (61). In particular, runs 11, 15, and 16 in Fig. 5 all have surface-augmented mixing and clearly exhibit the relatively thick boundary layer in $\overline{b}_z$. In this case the depth of the SDL, d defined in (66), is proportional to $\delta_s = 40$ m, and therefore also to $h_{\rm mix}$ in (59). This is confirmed in Fig. 7, which shows that in the runs with surface-augmented mixing d becomes independent of κ_a (and roughly of order 100 m) as $\kappa_a \to 0$ with fixed κ_s.

An explicitly modeled mixed layer has consequences on the total meridional transport so that the scaling for F_0 and D needs to be reevaluated. Integrating the buoyancy equation from the bottom of the mixed layer to the surface we find

$$F_0 \approx \kappa_a \overline{b}_z|_{z=-\delta_s} + \partial_y \left[\int_{-\delta_s}^{0} (\overline{\psi b}_z + \overline{v'b'})\, dz \right]. \tag{70}$$

This is the same expression as (68) except that now the depth of the SDL, d, coincides with δ_s. The first term on the right-hand side of (70) scales as the interior flux, and the vertical scale of $\overline{b}$ is given by the vertical scale of the thermocline, h, just as in the case of constant κ. The second term on the right-hand side of (70) can be estimated by assuming that within the mixed layer the eddy transport is of the same order as in the thermocline. Thus we find

$$F_0 = O(\kappa_a B/h) + O[\delta_s \tau B/(hfL_y)]. \tag{71}$$

Notice that the first term on the right depends on κ_a and might become smaller than the second term when κ_a is sufficiently small. Indeed, we see this in Fig. 7. With large abyssal diffusion, $\kappa_a = 8 \times 10^{-4}$ m^2 s^{-1}, d becomes comparable to the thermocline depth h, even though 8×10^{-4} m^2 s$^{-1} \ll \kappa_s$. Thus there is numerically significant κ_a correction to the ultimate scaling $d \propto \delta_s$ in the runs with the largest (unrealistic) values of κ_a.

Using (44) and (40) the specific scaling for Dh predicted by (71) is

$$Dh = O\left(\kappa_a \frac{L_y^2}{H}\right) + O\left(\delta_s \frac{\tau L_y}{fH}\right). \tag{72}$$

Figure 8 shows the quantity $D\,h$ as a function of κ_a for the runs in Tables 1 and 2. A constant, $D_{\rm mix} = 2.4 \times \delta_s \tau L_y/(fH)$ is subtracted from Dh for runs 6–16 (with surfaced enhanced diffusion) to test the scaling (71). The residual $D(h - h_{\rm mix}) - D_{\rm mix}$ shows a linear dependence on κ_a just as the computations with constant mixing. However, for the smallest values of κ_a the heat transport is dominated by the mixed layer contribution,

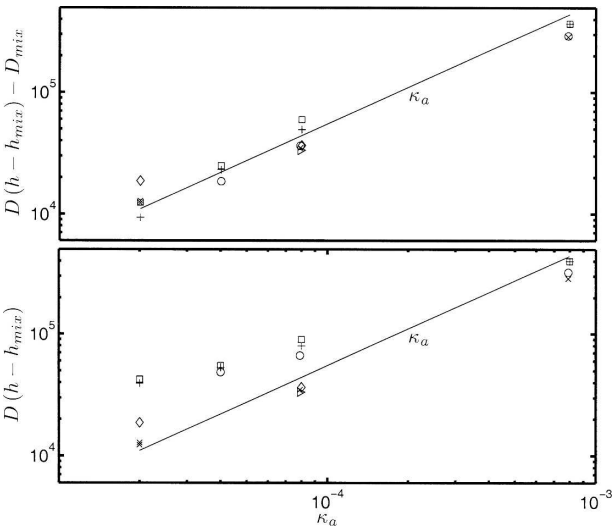

FIG. 8. Plot of $D(h - h_{\rm mix})$ as a function of κ_a. Runs 3 and 4 have the same value of κ_a, but different values of r, and yield the same value of $D(h - h_{\rm mix})$. (top) A constant $D_{\rm mix} = 2.4\delta_s \tau\, L_y/(2\pi fH)$ is subtracted for those runs with enhanced surface diffusion. According to the scaling (72), the additional transport of buoyancy in the mixed layer is independent of the diffusivity.

$D_{\rm mix}$, which is independent of the abyssal small-scale mixing, but depends on the mixed-layer depth.

9. Conclusions and discussion

One important result is (64), which states that the net meridional buoyancy transport (and thus the heat transport) is linearly proportional to the diffusivity, controlled by small-scale mixing. This is because the meridional buoyancy transport is proportional to the surface diffusive flux of buoyancy. Without the mediation of a mixed layer characterized by enhanced mixing over a depth scale δ_s, the thermocline depth scale is impressed onto the surface. For the arrangement of wind stress and surface buoyancy distributions that are typical of the ACC region, the depth of the thermocline is independent of the small-scale mixing: the vertical scale to which surface horizontal gradients are subducted is determined by a competition between mean and eddy buoyancy fluxes, and neither are controlled by small-scale mixing.

We find that the bulk of the meridional transport occurs in a thin layer near the surface, and it is thus not surprising that enhanced surface mixing has significant effects. For surface intensified mixing, the heat transport is increased and, when the abyssal diffusivity becomes small, is of order 1×10^{-5} m^2 s^{-1}, the buoyancy flux at the surface is dominated by the convergence of eddy transport within the mixed layer, whose vertical

scale is set by mixed layer processes. As a result, the total meridional transport becomes independent of the small-scale mixing coefficient, but is linearly proportional to the depth of the mixed layer. A similar result of weak interior meridional heat transport in the ACC, augmented by mixed layer processes, has been also found by Gallego et al. (2004). The notion that the mixed layer might be responsible for a larger fraction of the heat transport than the deep ocean on the global scale has also been advanced by Emanuel (2001).

We find that there are no substantial differences between a fixed and a relaxation boundary condition for the surface buoyancy. This is because the roughness depth, δ_*, is much less than the buoyancy depth scale, h, for typical values of the bulk transfer coefficient of heat, $\lambda \approx 40$ W m^{-2} K^{-1}. Equivalently, the relaxation time to the apparent atmospheric temperature is faster than the advection time due to the mean overturn, so the mean surface temperature is clamped to the specified distribution.

Although the depth of the thermocline is independent of the small-scale mixing, we find that it depends on the bottom drag because this is the main source of energy dissipation. Bottom drag controls the strength of the barotropic eddies, which are responsible for the eddy buoyancy flux. A similar result was also found in Cessi and Fantini (2004) in the context of a purely buoyancy-driven system. It is likely that the sensitivity to friction of the eddy statistics is reduced by the presence of planetary vorticity gradients and, possibly, by bottom relief. With planetary vorticity gradients, the flow in the ACC is structured in multiple jets maintained by eddy momentum fluxes (Sinha and Richards 1999): this is an indication that eddies do not grow to scales much larger than the deformation radius, a key assumption in our scaling.

With a mixed layer, typical values of the bulk diffusivity are small, $D \approx 200$ m^2 s^{-1}. We can use this value in (43) to estimate the heat transported in the ACC region as $c_p \rho H L_x D(dT_s/dy)$, where T_s is the surface temperature associated with the specified surface buoyancy. Using the values cited in Table 1, except that $L_x = 2 \times 10^7$ m (as appropriate for the ACC), we find a transport of about 0.5 PW. This value is in the range obtained by Trenberth et al. (2001) using top-of-the-atmosphere radiation measurements and atmospheric reanalyses. Without a mixed layer and for values of the diapycnal diffusivity of about 2×10^{-5} m^2 s^{-1}, the heat transport is one-half to one-third smaller, in agreement with the results of Gallego et al. (2004).

The linear dependence of the net heat transport (or equivalently of the interior residual streamfunction) on the strength of the diabatic terms (either κ_a or δ_s) is a consequence of homogenization of Ertel's potential vorticity on isopycnals in the quasi-adiabatic interior. This is in contrast with the hypothesis that the mixed layer produces potential vorticity gradients in the adiabatic interior, with an associated nonzero residual circulation (Olbers and Visbeck 2005; Marshall and Radko 2005, manuscript submitted to *Progress in Oceanography*). In our direct numerical simulations eddies homogenize potential vorticity both with and without a mixed layer. Other eddy-permitting computations in less idealized geometries indicate that this is a robust result (cf. Henning and Vallis 2005).

The inefficient heat transport of the homogenized interior implies that diabatic processes are confined to a surface diabatic zone, primarily controlled by baroclinic eddies, a result anticipated by Kuo et al. (2005).

Other geometrical arrangements of the domain and of the wind stress and surface temperature profiles might lead to qualitatively different scalings both for the depth of the thermocline and for the heat transport. At the moment, few systematic studies of these scalings in the presence of mesoscale eddies exist. There is no doubt that eddies are essential in the ACC. Whether they are important in closed and semienclosed regions is an open question that deserves further examination.

Acknowledgments. PC's and JAP's research was supported by the Office of Science (BER) of the U.S. Department of Energy through Grant DE-FG02-01ER63252, and WRY's research was supported by NSF OCE96-16017. We acknowledge the Center for Computational Sciences-Climate and Carbon Research (CCS-CCR) at Oak Ridge National Laboratory for computational resources used in support of this project.

APPENDIX

The Eddy Quasigeostrophic Potential Vorticity

The large eddies have a typical length scale l defined as the mixing length in (49). We assume the scale separation

$$l \ll L_y, \tag{A1}$$

and also that mean quantities, such as $\overline{b}$ and $\overline{v'b'}$, vary only over the large-scale L_y. Beneath the SDL the flow is adiabatic and the leading order terms in the eddy buoyancy equation are

$$b'_t + \overline{u}b'_x + u'b'_x + v'b'_y + v'\overline{b}_y + w'\overline{b}_z \approx 0. \tag{A2}$$

The vertical component of the eddy vorticity equation is

$$\zeta'_t + \overline{u}\zeta'_x + u'\zeta'_x + v'\zeta'_y \approx fw'_z, \tag{A3}$$

where $\zeta' \equiv v'_x - u'_y$.

The quasigeostrophic eddy potential vorticity is

$$q' = \zeta' + f(b'/\overline{b}_z)_z. \tag{A4}$$

Eliminating w' between (A2) and (A3) we have[A1]

$$q'_t + \overline{u}q'_x + u'q'_x + v'q'_y + v'(\overline{b}_y/\overline{b}_z)_z = 0. \tag{A5}$$

If the zonally averaged buoyancy has homogeneous potential vorticity, then $(\overline{b}_y/\overline{b}_z)_z = 0$; that is, the final term on the lhs of (A5) vanishes. In this case there is no source of q' in (A5) and consequently $q' = 0$ (Rhines and Young 1982). The numerical computations summarized in Table 1 do indeed confirm that $q' = 0$ in the quasiadiabatic interior.

It is interesting that the eddy Ertel potential vorticity,

$$\pi' \approx \overline{b}_z\zeta' + fb'_z, \tag{A6}$$

satisfies

$$\pi'_t + \overline{u}\pi'_x + u'\pi'_x + v'\pi'_y + v'\overline{\pi}_y + w'\overline{\pi}_z = 0, \tag{A7}$$

where $\overline{\pi} = f\overline{b}_z$. Even with homogenized potential vorticity [i.e., $\overline{\pi}(y, z)$ uniform on $\overline{b}(y, z)$ surfaces] one generally has nonzero $\overline{\pi}_y$ and $\overline{\pi}_z$. Thus the sources in (A7) are nonzero, and so is π'.

Last, suppose that

$$R \ll l, \tag{A8}$$

where $R \approx \sqrt{Bh}/f$ is the Rossby radius. In this large-scale limit, the Reynolds stress divergence in the Charney–Drazin identity

$$\overline{v'q'} = -\overline{u'v'}_y + f(\overline{v'b'}/\overline{b}_z)_z \tag{A9}$$

is negligible. Then, since $q' = 0$ implies $\overline{v'q'} = 0$, one has

$$\overline{v'b'} = \phi(y)\overline{b}_z, \tag{A10}$$

where $\phi(y)$ is a constant of integration.

[A1] In the elimination, $\overline{b}_z(y, z)$ varies with y on the scale $L_y \gg l$ so that $v'b'_y/\overline{b}_z \approx v'(b'/\overline{b}_z)_y$. Also, because both mean and eddies satisfy the thermal wind relation, there is an important exact cancellation $\overline{u}_z(b'/\overline{b}_z)_x + v'_z(\overline{b}_y/\overline{b}_z) = 0$.

REFERENCES

Andrews, D., and M. McIntyre, 1976: Planetary waves in horizontal and vertical shear: The generalized Eliassen–Palm relation and the mean zonal acceleration. *J. Atmos. Sci.,* **33,** 2031–2048.

Cenedese, C., J. Marshall, and J. Whitehead, 2004: A laboratory model of the thermocline depth and exchange fluxes across circumpolar fronts. *J. Phys. Oceanogr.,* **34,** 656–667.

Cessi, P., and M. Fantini, 2004: The eddy-driven thermocline. *J. Phys. Oceanogr.,* **34,** 2642–2658.

Emanuel, K., 2001: Contribution of tropical cyclones to meridional heat transport by the oceans. *J. Geophys. Res.,* **106,** 14 771–14 781.

Gallego, B., P. Cessi, and J. C. McWilliams, 2004: The Antarctic Circumpolar Current in equilibrium. *J. Phys. Oceanogr.,* **34,** 1571–1587.

Gill, A. E., J. S. A. Green, and A. J. Simmons, 1974: Energy partition in the large-scale ocean circulation and the production of mid-ocean eddies. *Deep-Sea Res.,* **21,** 499–528.

Green, J., 1970: Transfer properties of the large-scale eddies in the general circulation of the atmosphere. *Quart. J. Roy. Meteor. Soc.,* **96,** 157–185.

Haney, R. L., 1971: Surface thermal boundary condition for ocean circulation models. *J. Phys. Oceanogr.,* **1,** 241–248.

Henning, C., and G. Vallis, 2005: The effects of mesoscale eddies on the stratification and transport of an ocean with a circumpolar channel. *J. Phys. Oceanogr.,* **35,** 880–896.

Johnson, G., and H. Bryden, 1989: On the size of the Antarctic Circumpolar Current. *Deep-Sea Res.,* **36,** 39–53.

Karsten, R., H. Jones, and J. Marshall, 2002: The role of eddy transfer in setting the stratification and transport of a circumpolar current. *J. Phys. Oceanogr.,* **32,** 39–54.

Kuo, A., A. Plumb, and J. Marshall, 2005: Transformed Eulerian-mean theory. Part II: Potential vorticity homogenization, and the equilibrium of a wind- and buoyancy-driven zonal flow. *J. Phys. Oceanogr.,* **35,** 175–187.

Larichev, V. D., and I. M. Held, 1995: Eddy amplitudes and fluxes in a homogeneous model of fully developed baroclinic instability. *J. Phys. Oceanogr.,* **25,** 2285–2297.

Marshall, J., and T. Radko, 2003: Residual-mean solutions for the Antarctic Circumpolar Current and its associated overturning circulation. *J. Phys. Oceanogr.,* **33,** 2341–2354.

——, D. Olbers, H. Ross, and D. Wolf-Gladrow, 1993: Potential vorticity constraints on the dynamics and hydrography of the Southern Ocean. *J. Phys. Oceanogr.,* **23,** 465–487.

——, C. Hill, L. Pereleman, and A. Adcroft, 1997a: Hydrostatic, quasi-hydrostatic, and nonhydrostatic ocean modeling. *J. Geophys. Res.,* **102,** 5733–5752.

——, A. Adcroft, C. Hill, and L. Pereleman, 1997b: A finite-volume, incompressible Navier-Stokes model for studies of the ocean on parallel computers. *J. Geophys. Res.,* **102,** 5753–5766.

——, H. Jones, R. Karsten, and R. Wardle, 2002: Can eddies set ocean stratification? *J. Phys. Oceanogr.,* **32,** 26–38.

Munk, W., and C. Wunsch, 1998: Abyssal recipes. II. Energetics of tidal and wind mixing. *Deep-Sea Res. I,* **45,** 1977–2010.

Olbers, D., and M. Visbeck, 2005: A model of the zonally averaged stratification and overturning in the Southern Ocean. *J. Phys. Oceanogr.,* **35,** 1190–1205.

Paparella, F., and W. R. Young, 2002: Horizontal convection is non-turbulent. *J. Fluid Mech.,* **466,** 205–214.

Pedlosky, J., 1987: *Geophysical Fluid Dynamics*. 2d ed. Springer Verlag, 710 + xiv pp.

Plumb, R. A., and R. Ferrari, 2005: Transformed Eulerian mean theory. Part I: Nonquasigeostrophic theory for eddies on a zonal-mean flow. *J. Phys. Oceanogr.,* **35,** 165–174.

Rhines, P. B., 1977: The dynamics of unsteady currents. *The Sea,* E. D. Goldberg, Ed., John Wiley and Sons, 189–318.

——, and W. R. Young, 1982: Homogenization of potential vorticity in planetary gyres. *J. Fluid Mech.,* **122,** 347–367.

Riviere, P., A. M. Treguier, and P. Klein, 2004: Effects of bottom friction on nonlinear equilibration of an oceanic baroclinic jet. *J. Phys. Oceanogr.,* **34,** 416–432.

Salmon, R., 1980: Baroclinic instability and geostrophic turbulence. *Geophys. Astrophys. Fluid Dyn.,* **15,** 165–211.

Sinha, B., and K. Richards, 1999: Jet structure and scaling in Southern Ocean models. *J. Phys. Oceanogr.,* **29,** 1143–1155.

Smith, K. S., G. Boccaletti, C. C. Hennings, I. Marinov, C. Y. Tarn, I. M. Held, and G. K. Vallis, 2002: Turbulent diffusion in the geostrophic inverse cascade. *J. Fluid Mech.,* **469,** 13–48.

Stommel, H., 1961: Thermohaline convection with two stable regimes of flow. *Tellus,* **13,** 224–230.

Thompson, A. F., and W. Young, 2005: Scaling baroclinic eddy fluxes: Vortices and energy balance. *J. Phys. Oceanogr.,* **36,** 720–738.

Trenberth, K., J. Caron, and D. Stepaniak, 2001: The atmospheric energy budget and implications for surface fluxes and ocean heat transports. *Climate Dyn.,* **17,** 259–276.